

S1222a - the largest Marsquake detected by InSight

Taichi Kawamura¹, John F. Clinton², Géraldine Zenhäusern³, Savas Ceylan³, Anna C. Horleston⁴, Nikolaj L. Dahmen³, Cecilia Duran³, Doyeon Kim³, Matthieu Plasman¹, Simon C. Stähler³, Fabian Euchner³, Constantinos Charalambous⁵, Domenico Giardini³, Paul Davis⁶, Grégory Sainton¹, Philippe Lognonné¹, Mark Panning⁷, William B. Banerdt⁷

¹Université Paris Cité, Institute de physique de globe de Paris, CNRS, Paris, France

²Swiss Seismological Service, ETH Zurich, Zurich, Switzerland

³Institute of Geophysics, ETH Zurich, Zurich, Switzerland

⁴School of Earth Sciences, University of Bristol, Bristol, UK

⁵Imperial College London, London, UK

⁶University of California, Los Angeles, USA

⁷Jet Propulsion Laboratory, Pasadena, USA

Key Points:

- InSight detected on May, 4, 2022 a $M_W^{Ma} 4.7$ marsquake, S1222a, which is the largest seismic event detected so far.
- The exceptional signal-to-noise allows multiple phases to be identified, with a rich collection of surface waves.
- S1222a was located 37 degrees southeast of the InSight landing site and close to the Martian dichotomy boundary.

Corresponding author: Taichi Kawamura, kawamura@ipgp.fr

This article has been accepted for publication and undergone full peer review but has not been through the copyediting, typesetting, pagination and proofreading process, which may lead to differences between this version and the [Version of Record](#). Please cite this article as [doi: 10.1029/2022GL101543](https://doi.org/10.1029/2022GL101543).

This article is protected by copyright. All rights reserved.

21 Abstract

22 NASA's InSight has detected a large magnitude seismic event, labelled S1222a. The event
 23 has a moment magnitude of $M_W^{Ma} 4.7$, with 5 times more seismic moment compared to
 24 the second largest even. The event is so large that features are clearly observed that were
 25 not seen in any previously detected events. In addition to body phases and Rayleigh waves,
 26 we also see Love waves, minor arc surface wave overtones, and multi-orbit surface waves.
 27 At long periods, the coda event exceeds 10 hours. The event locates close to the North-
 28 South dichotomy and outside the tectonically active Cerberus Fossae region. S1222a does
 29 not show any evident geological or tectonic features. The event is extremely rich in fre-
 30 quency content, extending from below 1/30 Hz up to 35 Hz. The event was classified as
 31 a broadband type event; we also observe coda decay and polarization similar to that of
 32 very high frequency type events.

33 Plain Language Summary

34 After 3 years of seismic monitoring of Mars by InSight SEIS instrument, we detected
 35 a marsquake largest ever observed during the mission. The event is larger by factor of
 36 5 in seismic moment compared to previously detected events. With such an energetic
 37 event, we discovered various seismic features that was never observed before. For the first
 38 time, we were able to detect body waves and surface waves with their overtones. The
 39 large variety of detected seismic phases will enable us to probe the internal structure of
 40 Mars. Secondly, the event was located outside a well-known seismically active region of
 41 Cerberus Fossae. This might indicate that that event do not come from the same fault
 42 system with other major marsquakes. Finally, this event shows simultaneously features
 43 of marsquakes that were previously classified into different types. S1222a is classified as
 44 a broadband event with a wide frequency range of seismic energy. At the same time, the
 45 coda shape and decay at high frequency resembles that of very high frequency type events.
 46 It was an open question how different types of marsquakes are excited of what makes
 47 such differences and such event will be a key to uncover such mystery of marsquakes.

48 1 Introduction

49 NASA's Interior Exploration using Seismic Investigations, Geodesy and Heat Trans-
 50 port (InSight) mission has achieved almost continuous seismic monitoring of Mars since
 51 early 2019 (Banerdt et al., 2020; Lognonné et al., 2020). Since May 2022, the local back-
 52 ground seismic noise has increased due to the typical atmospheric disturbance observed
 53 during the Martian autumn and winter, and the power situation had deteriorated to the
 54 point that InSight's SEIS (Seismic Experiment for Interior Structure) instrument (Lognonné
 55 et al., 2019) was about to begin to be periodically switched off. In this challenging sit-
 56 uation, SEIS recorded the largest marsquake ever detected during the mission lifetime
 57 to date. On May 4th, at 23:23:07 UTC, also known as the 1222nd Martian day (sol) since
 58 InSight landed, a magnitude $M_W^{Ma} 4.7$ marsquake shook the red planet. The aim of this
 59 paper is to describe in detail the main characteristics of the event and provide initial con-
 60 text for further research.

61 To uncover the internal structure of Mars, InSight was equipped with a suite of geo-
 62 physical instruments and seismic sensors; SEIS is one of the key scientific instruments
 63 of the mission (Banerdt et al., 2020; Lognonné et al., 2019; Lognonné et al., 2020). Since
 64 the deployment, SEIS has been monitoring Martian seismicity for more than 1350 sols
 65 (each sol is approximately 24h39m). SEIS consists of two seismometers, the Very Broad-
 66 band (VBB) seismometer and the Short Period (SP) seismometer designed to cover the
 67 different frequency bands. InSight also has a series of environmental monitoring sensors
 68 known as the Auxiliary Payload Sensor Suite (APSS). APSS includes meteorological sen-
 69 sors (pressure, wind and thermal sensors) and a magnetometer (Banfield et al., 2019, 2020;
 70 Johnson et al., 2020). SEIS data are strongly contaminated by environmental, spacecraft

and instrumental noise (Ceylan et al., 2021; Scholz et al., 2020; Kim, Davis, et al., 2021). In the nominal configuration, InSight simultaneously observes both seismic signals and environmental noise, which allows seismologists to distinguish between true seismic events and environmental noise injection (Clinton et al., 2021; Charalambous et al., 2021). However, this was no longer possible since Sol 789 due to power limitations that required shutting down of some of the scientific payload. The two solar panels that are used to power the spacecraft and the instrument have been steadily accumulating Martian dust and the power generation has degraded significantly. Thus, for the last 600 sols, SP and APSS were only occasionally powered on and only the VBB has been powered on continuously, with sampling at 20 Hz. Neither the SP nor APSS were turned on during S1222a. VBB was operating in high-sampling-rate mode and it was possible to also retrieve 100 Hz for the event. SEIS data is archived and released by InSight Mars SEIS Data Service and the data is available to the science community with 3 months delay (InSight Mars SEIS Data Service, 2019).

Using InSight seismic data, various Martian seismic velocity models were proposed (Giardini et al., 2020; Lognonné et al., 2020; Stähler et al., 2021; Khan et al., 2021; Knapmeyer-Endrun et al., 2021; Kim, Lekić, et al., 2021; Drilleau et al., 2021, 2022). The Marsquake Service (MQS), who delivers the marsquake catalog to the community, uses the suite of models proposed in Stähler et al. (2021) to locate seismic events. This approach was proven to be highly plausible after the remarkable precision we achieved for detected impacts whose locations were confirmed using orbital imaging (Garcia et al., 2022; Posiolova et al., 2022). Back azimuths are obtained based on the method described in Zenhäusern et al. (2022). This method provides a more rigorous and systematic estimation of the polarization compared to the former approach described in Böse et al. (2017), not least since it combines observations from both P and S arrivals. Its efficacy was also demonstrated through analyses of ambient noise (Stutzmann et al., 2020). Event depths are challenging to define using only a single station where depth phases are rarely identified, so MQS assigns a fixed depth of 50 km to all events.

2 Event Overview

Figure 1 and Table 1 show the general characteristics of event S1222a and the context of the background environmental noise. Waves from the event first reached InSight shortly before 4AM Local Mean Solar Time (LMST) on Mars. S1222a occurred in mid-autumn at the landing site, a season with high seismic noise due to persistent winds. Broadband noise injection from wind was observed constantly before and during the event as evidenced by the presence of clear lander resonances (Dahmen et al., 2021; Charalambous et al., 2021). In addition to the environmental noise, InSight data suffers from glitches which are likely due to thermal-induced shocks within the instrument or the lander (Scholz et al., 2020). Glitches are 1-sided pulses that can be modelled by the instrument response to a step in acceleration, and hence appear as near-critically damped 20s signals, that are rich in all frequencies. The signals regularly corrupt the seismic signal and obscure phase interpretation (Kim, Davis, et al., 2021). Despite the very high amplitude seismic signals, strong glitches are present throughout S1222a. To avoid misinterpretation of seismic phases with glitches, analysis of the data is performed on both raw data as well as deglitched data following the methods described in Scholz et al. (2020).

Despite the high background noise, the seismic energy of the event strongly exceeds the noise level (Figure1(d)). The event is rich in frequency content and for many minutes following the energy onset, signal far exceeds the noise level from below 30 seconds to 35 Hz. Comparing the seismic spectra to the background noise, the signal to noise ratio is as high as 40 dB at ~30 seconds and 60 dB at ~1Hz (Figure1(d)). Following the MQS convention, since there is very significant energy below 2.4 Hz, the event is catalogued as a Broadband (BB). This event is remarkable in many ways - low-frequency energy persists for approximately 10 hours (Figure1(b)). While the high frequency energy

above 1 Hz attenuates far more rapidly (~ 20 min) than the long period one, the resonance at 2.4 Hz continues to ring for an additional (~ 20 min). The origin of the resonance is not yet clear but the prominent peak is used to distinguish and discriminate different types of marsquakes (Clinton et al., 2021; Ceylan et al., 2022). Previously, no broadband event included energy above 10 Hz, yet in S1222a energy is clearly present up to 35 Hz and is strongest on the horizontal components at high frequencies - behaviour that otherwise is only observed in Very High Frequency (VF) events. The event spectrum is so broad and large it spans all previously known event types.

The peak amplitude of the signal reaches 2.8×10^{-5} m/s on the instrument-response-corrected radial components. On the oblique components of the raw data, the value is 2.4×10^{-5} m/s, equivalent to 2.2 millions counts. It is noted that this is 26% of the 2^{23} count limit of the 24-bit EBOX digitiser (Zweifel et al., 2021). SEIS was remarkably close to saturation during this event.

2.1 Phase Identification

Two energy packets can be clearly identified that are interpreted as P and S body waves, as has been done for other Low Frequency family events (Clinton et al., 2021; Ceylan et al., 2021)(Figure1(e)). The onset of each packet is picked as the first arrival of each phase. The P coda has almost constant amplitude across the minutes before the S arrival. After the arrival of the stronger S phase, energy gradually decays which is a typical characteristic of the High Frequency family of marsquakes (Figure1(e)).

In addition to the routinely identified body phases, surface waves are clearly visible in the S-wave coda (Figure1(a,b,c)). To date, the only surface waves identified on Mars have been fundamental Rayleigh waves that were observed in 2 other events, S1000a and S1094b (Kim et al., 2022). In the case of S1222a, a much richer set of surface waves are observed. Both fundamental Rayleigh and Love waves (R1 and G1 respectively), and first overtones (R1_1 and G1_1), can be identified. Further, major arc R2 and multi orbit R3, although weak, can be identified, and there are suggestions of later multi-orbit arrivals (x4, x5). All the phase arrival picks that were made by MQS are summarized in Table 1. We will describe in detail in the following the phases that we identified.

2.1.1 Body Waves

The first clear arrival visible in the data is an impulsive P wave. The P arrival was picked in the time domain which is only possible for events with a high signal-to-noise ratio, such as 14 quality A events. 1.5-10 seconds filtered data were used to identify the downward motion of the P arrival with an uncertainty of 0.5 seconds. In Figure 2 we can see a clear impulsive and broadband P arrival between 3 Hz - 10 s, though above 3 Hz there is a distinct delay in arrival time that increases linearly with frequency, possibly the effect of scattering at higher frequencies. The P arrival is glitch free though a large glitch is observed within the P coda (obvious glitches are indicated in the timeseries shown in Figure 1(e,f)). Polarisation analysis (see below) shows that this phase is strongly and persistently polarised. A stronger second envelope of energy arrives approximately 3.5 min later, consistent with an S phase arrival. The polarisation is persistent and different to the P-wave, allowing us to label it as a S-phase (Figure3). The impulsive S arrival can also be identified in the time series, for the MQS phase pick we used data filtered between 1.5 and 10 seconds, and assigned a 2 seconds uncertainty. As in the case for P wave, the S wave also shows an impulsive broadband arrival though is similarly delayed at higher frequencies. A large number of significant glitches are present in the S-wave coda, though they are not clearly visible in the raw time series since the signal amplitudes are so high - they are revealed if the signal is integrated to displacement.

Both the P and S wave coda include high frequency energy that reaches up to \sim 32.5 Hz with signal to noise ratio larger than 10(Figure 2). In order to be consistent with other broadband events in the catalogue, MQS also identified y1 and y2 arrivals which correspond to the arrival times of the high frequency portion of the energy and are picked using the energy envelope at the 2.4Hz resonance (Ceylan et al., 2021). As expected, arrivals are very similar to the P and S arrivals, lying within the error bars, as shown in Table 1. As for other VF events, S1222a has stronger horizontal energy at high frequencies and the horizontal energy persists to higher frequencies while the vertical energy decays quickly (Figure 1(c,d))(van Driel et al., 2021; Menina et al., 2021; Karakostas et al., 2021).

2.1.2 Surface Waves

Almost no other marsquake had energy above the noise below 10s. At periods from about 10-30 seconds, S1222a exhibits dispersive signals which are a strong indication of surface waves. Surface waves were first reported for two large impacts where the surface source efficiently excited surface waves (Kim et al., 2022). The polarised P-wave allows us to rotate the signal into radial and transverse components, aiding our interpretation. For S1222a, on the vertical and radial components, we see a clear Rayleigh wave between at least 10 and 35 seconds period, starting about 4.5 minutes after the S arrival (Figure1(f)). As shown in Table 1 and visible in Figure1(c), the signal shows clear dispersion where phase arrivals are delayed towards the high frequencies. Furthermore, we can also identify a first overtone arriving before the fundamental mode. The overtone is shifted towards the higher frequencies and the dispersive signal is detected in the period range of 3 - 15 seconds. In addition to the Rayleigh wave, on the transverse component, a Love wave was detected for the first time on Mars for S1222a at 23:33:38.2, which is about 2 minutes after the S arrival. The strong signal dominantly observed on the transverse component is a strong indication of a Love wave and this was interpreted as a fundamental Love wave. The Love wave arrives about 2.5 minutes before the Rayleigh wave and almost at the same time as the Rayleigh wave overtone. Given that this is unique observation we have for S1222a, these surface waves are used to investigate the Martian structure (e.g. Beghein et al., submitted; Li et al., submitted; Kim et al., submitted).

2.2 Multi-orbit Surface Waves

S1222a not only enabled us to identify Love waves for the first time on Mars, it also provides us with opportunities to explore further subsequent surface waves. In Figure 1(a), where we plot a 12 hour spectrogram in acceleration, we see energy significantly higher than the background noise at 01:15(UTC). The signal shows a weak dispersion but this is difficult to confirm with the low signal to noise ratio. The energy is followed by another packet of energy about 20 minutes later. This signal is overlapping with a significant glitch but is clearly visible after the deglitching (Figure1(a)). These signals are only visible in the vertical component and this makes it difficult for us to investigate the polarization of these signals. However, given the dispersive feature of the signal, we concluded that these are the R2 and R3 phases and their picks are also provided in Table1. Similar multi-orbit phases were not identified for Love waves which is reasonable given the higher noise level on the horizontal components, where Love waves should be most visible. This is the first time that we have identified and catalogued R2 and R3.

2.3 Distance Analysis

As done throughout the mission, we used P and S arrivals and a suite of reference seismic velocity models (Stähler et al., 2021) to find the most probable location (modified after (Böse et al., 2017)). This provides a distance consistent with all the other events in the catalog (Ceylan et al., 2021) and we are confident that this gives us a reasonable

distance after the detection of confirmed impacts (Posiolova et al., 2022). This gave us 37 degrees for the distance. We refrain from using fundamental and overtone surface wave arrival times here since our methods are not yet calibrated for these phases.

Our pre-landing plan was to use R1/2/3 to locate marsquakes with a single station. This method was described in various pre-landing papers but was not used to date given the lack of R2/R3 detection (Panning et al., 2015; Böse et al., 2017; van Driel et al., 2019). Given that this is our first detection of R2 and R3, we tested this method to locate the marsquake and compared with the distance obtained from the body waves. With R1/2/3, we obtained 35.4 degrees which is consistent and overlaps with the value obtained with body waves within the range of the errorbar. More detailed discussion on the source location using R1/R2/R3 can be found in Panning et al. (submitted). While S1222a enabled us to at last confirm our pre-landing concept, we did not include this as the preferred location for consistency with other events in the catalog.

2.4 Back-azimuth Analysis

Figure 3(a) shows the result of the back azimuth analysis for body waves by using the eigenvector method described in Zenhäusern et al. (2022) and adopted by MQS from catalog V12. Data here includes a linearity filter to accentuate body wave energy, which is defined as $F_e = (1 - \epsilon)^2$. ϵ is the ellipticity of the signal and is 0 for a rectilinear and 1 for a circular signal (for details see Zenhäusern et al. (2022)). The P energy observed between 1/10-1/2 Hz, the window MQS uses to determine LF family polarization, has a polarization that peaks at 101 degrees. This value is consistent over a wide frequency band, from 1/10 to 2 Hz and time window (shown in yellow in Figure 3(a)). As is normal for marsquakes, high frequency energy is intensely scattered. The incident angles of about 70-80 degrees (shown in orange in the figure) are observed at 1/5-1/2 Hz. Such vertical polarization supports our identification of the P wave. When we focus on the S wave, we also see coherent energy around a similar frequency band as the P wave which clearly has a different back-azimuth of about 0°, about 90° shifted from the P polarization, and having a low inclination angle of about 20°. Both are consistent with an S-wave.

Figure 3(b) shows the same polarization analyses, but without linearity filter, in order to accentuate surface wave energy. Indicated in the figure both the fundamental Rayleigh (green ellipse) and Love (light blue ellipse) wave energy are indicated. The Rayleigh wave is visible with a high ellipticity signal. The back azimuth obtained from the Rayleigh wave is similar but offset from that obtained from body waves and is estimated to be about 120°. The Love wave has horizontal polarization as expected from a typical Love wave. In contrast to the Rayleigh wave, it has a rectilinear, meaning the signal is linear. From both body waves and surface waves, we have a self-consistent set of polarization. To be consistent with the MQS catalogue, the preferred back azimuth is 101° (96°-112°).

2.5 Location of S1222a

Combining the distance and the back azimuth, the event can be located at 3.0°S, 171.9°E (Figure 3(c), Table 1). The uncertainty ellipse is indicated in the figure, dominated by the relatively wide uncertainty in backazimuth. The event appears to lie about 10° to the south of the farthest Eastern extent of Cerberus Fossae, by a considerably margin the most seismically active region on Mars (Giardini et al., 2020; Perrin et al., 2022; Rivas-Dorado et al., 2022; Zenhäusern et al., 2022; Stähler et al., 2022). The majority of located seismic events locate within this region (Ceylan et al., 2022) and a clear link between the surface fault system and source mechanisms is suggested (Brinkman et al., 2021; Jacob et al., 2022). S1222a locates in a region closer to the North-South dichotomy (Smith et al., 2001). Unlike the Cerberus Fossae region, the epicenter of S1222a shows no evident tectonic features. In addition, no new crater of appropriate size has been de-

270 tected in orbital images taken of the location error ellipse, thus far. Further investigation
271 should be done with higher resolution imagery (e.g. MRO HiRISE).

272 2.6 Magnitude Evaluation

273 Following the methods described in (Böse et al., 2021), we obtained magnitudes
274 for this event, which are summarized in Table 1. We assigned 3 types of magnitude de-
275 pending on the frequency band and the method that we use to define the magnitude. The
276 first, $M_{w,\text{spec}}^{\text{Ma}}$ was defined using the body wave spectrum and fitting this with omega square
277 model. We obtained 4.7 ± 0.2 for the magnitude which is larger by 0.5 compared to the
278 second largest event ($S0976a, M_{w,\text{spec}}^{\text{Ma}} = 4.2 \pm 0.3$ (Horleston et al., 2022)). This was viewed
279 as the reference magnitude among the obtained magnitudes and was used to calculate
280 the seismic moment. This magnitude is by far the largest of all the catalogued marsquakes
281 and the seismic moment release of this single event is comparable to all other events in
282 the marsquake catalog combined. The other two magnitudes were calculated from body
283 wave amplitudes for P and S filtered at 2–6 seconds period. The body wave magnitude
284 (m_b^{Ma} and $m_b S^{\text{Ma}}$) was obtained from P and S amplitude respectively and we obtained
285 5.3 and 5.8. The difference in the obtained magnitude can be explained by the high cor-
286 ner frequency compared to other marsquakes, which was generally observed for marsquakes
287 outside Cerberus Fossae region (Stähler et al., 2022).

288 2.7 Spectral analysis

289 S1222a shows one of the richest frequency contents ever seen for marsquakes with
290 a significantly wider frequency band that ranges from 1/30 Hz to 35 Hz, compared to
291 previously detected events. Both P and S arrivals have broadband energy covering fre-
292 quencies as low as ~ 0.02 Hz up to ~ 35 Hz (Figure 1(c), Figure 2). The noise starts to
293 increase below ~ 0.4 Hz and becomes dominant at ~ 0.01 Hz. The S wave extends over
294 a wider frequency band, covering both lower and higher frequencies compared to the P
295 wave. At high frequencies above 1 Hz, the P and S waves have similar spectral shapes
296 that almost overlap with each other.

297 When we compare spectra from the vertical and horizontal components, we see clear
298 enhancement for horizontal components (Figure 1(c)). While the spectrum of the ver-
299 tical component decays rapidly with frequency, the horizontal components show almost
300 flat or slightly decaying spectra. This is a typical characteristic observed for VF type events.
301 Such a feature was not observed for other BB type events. At frequencies higher than
302 1 Hz, we see a characteristic peak centered around 2.4 Hz. The resonance at 2.4 Hz is
303 widely known and was reported in previous studies (van Driel et al., 2021; Dahmen et
304 al., 2021; Hobiger et al., 2021). The high corner frequency of the event is unusual for other
305 relatively large marsquakes, specifically those observed in Cerberus Fossae (Stähler et
306 al., 2022), and suggests that the event occurs outside this fault system, which is consis-
307 tent with the location we obtained.

308 3 Discussion

309 3.1 Possible Aftershock

310 About 34 hours after S1222a, a small VF event was detected (S1223a). While this
311 was a much weaker event compared to S1222a ($M_W^{\text{Ma}} = 2.9$), the event was carefully ex-
312 amined given the possibility of it being an aftershock of S1222a. S1223a clearly lacks long
313 period energy compared to S1222a, thus it is catalogued as a VF event and not a BB event.
314 This is unlikely for an aftershock but this might be due to the large difference in the mag-
315 nitudes of the two events. Due to strong environmental noise injection at the time of S1223a,
316 the time differences between the P and S arrivals were constrained through comodula-
317 tion from weather-sensitive lander resonances (Charalambous et al., 2021) and indicate

318 similar time delays for both events (3 minutes 20 seconds and 3 minutes 34 seconds). As
 319 is often the case for VF events, no polarization can be assigned.

320 3.2 Additional Multi-orbit Phases

321 S1222a is so large that beyond the multi-orbit R3 phase arrival there are hints for
 322 further phase arrivals, which are labelled in Figure1 and Table 1 as x4 and x5. The pre-
 323 landing expectation was that locations could be made using any combination of body
 324 phases and surface waves. In the pre-launch blind test (Clinton et al., 2017; van Driel
 325 et al., 2019), source locations were tested using body waves and R1/R2/R3. Further multi-
 326 orbit phases were not considered or their utilisation was not tested (Panning et al., 2015;
 327 Böse et al., 2017). However, for S1222a, we were able to identify some increases in en-
 328 ergy on the vertical component at around the expected time windows for R4 and R5. The
 329 signal to noise ratio is low and we were not able to see any clear dispersive phase in the
 330 data, leaving some uncertainties in their identification as R4 and R5. Thus, we included
 331 these signals in the catalog as x4 and x5, using the indicator x, which MQS uses for un-
 332 known phases. While we would like to let future studies to confirm this, we believe that
 333 these arrivals are possible candidates for R4 and R5.

334 4 Conclusion

335 We reported in this study the general characteristics of S1222a, the magnitude 4.7
 336 marsquake located 37°distance from the SEIS seismometer, which is by far the largest
 337 event detected during the InSight mission to date. Both body waves and a rich suite of
 338 surface waves can be identified, including both fundamental and first overtone Rayleigh
 339 and Love waves, and multi orbit Rayleigh waves. As recorded at InSight, the event in-
 340 cludes energy ranging from below 1/30 Hz up to 35Hz. In the context of the marsquake
 341 catalog event types, the low frequency component (<2.4Hz) resembles broadband type
 342 events whereas the higher frequency component is characteristic of very high frequency
 343 events. Such an event may provide us with a clue to understand the different types of
 344 marsquakes and their origins. The event is located close to the North/South dichotomy
 345 of Mars and outside the well-known Cerberus Fossae region where many of the major
 346 seismic events are located. These features require further investigation and the event will
 347 serve as an unique example to uncover the mysteries of Martian seismicity.

348 Acknowledgments

349 We acknowledge NASA, CNES, partner agencies and institutions (UKSA, SSO, DLR,
 350 JPL, IPGP-CNRS, ETHZ, ICL, MPS-MPG), and the operators of JPL, SISMOC, MSDS,
 351 IRISDMC and PDS for providing SEED SEIS data. Marsquake Service (MQS) opera-
 352 tions at ETH are supported by ETH Research grant ETH-06 17-02. ETH authors recog-
 353 nise support from the ETH+ funding scheme (ETH+02 19-1: “Planet Mars”). French
 354 co-authors acknowledge support of the French Space Agency CNES and Agence Nationale
 355 de la Recherche, ANR (ANR-19-CE31-0008-08). TK, MP, PL, GS acknowledge support
 356 of IdEx Université Paris Cité ANR-18-IDEX-0001. A.H. is funded by the UK Space Agency
 357 under grant numbers ST/R002096/1 and ST/W002523/1. This research was carried out
 358 in part at the Jet Propulsion Laboratory, California Institute of Technology, under a con-
 359 tract with the National Aeronautics and Space Administration (80NM0018D0004). This
 360 paper is InSight Contribution Number 285.

361 Open Research

362 All raw waveform data is available through the InSight Mars SEIS Data Service
 363 @ IPGP, IRIS-DMC and NASA PDS. (InSight Mars SEIS Data Service, 2019).

Table 1: General information of S1222a and Phase Picks from MQS

| | | |
|---|------------|---|
| Event parameters | Event name | S1222a |
| Origin time | | |
| UTC | 2022-05-04 | 23:23:07 ± 4.8s |
| LMST | | 03:54:39 |
| Distance | | 37° (±1.6°) |
| Backazimuth | | 101° (96°–112°) |
| Source Location | | 3.0 °S, 171.9 °E |
| M_w^{Ma} ($M_{w,\text{spec}}^{\text{Ma}}$) | | 4.7 ± 0.2 |
| m_b^{Ma} | | 5.3 |
| m_{bS}^{Ma} | | 5.8 |
| Seismic Moment (N.m) | | 1.4×10^{16} (7.0×10^{15} ~ 2.8×10^{16}) |
| Peak amplitude (m/s) | | |
| Vertical | | 1.3×10^{-5} |
| North | | 2.8×10^{-5} |
| East | | 2.8×10^{-5} |
| SNR (Seismic) | | 545194.7 |
| Duration | | ~633 min |

| Phase Arrivals | | |
|----------------|--|--------------------------------|
| Body waves | | |
| P | | 23:27:45.8 (±0.5 s) |
| S | | 23:31:20.1 (±2 s) |
| y1 | | 23:27:46.3 (±0.5 s) |
| y2 | | 23:31:30.8 (±10 s) |
| Surface waves | | |
| R1 | | |
| 1/34 Hz | | 23:35:59.1 (±20 s) |
| 1/28 Hz | | 23:35:58.3 (±20 s) |
| 1/24 Hz | | 23:36:14.3 (-50.2 ~ +42.0 s) |
| 1/20 Hz | | 23:36:27.9 (±43.4 s) |
| 1/17 Hz | | 23:36:48.2 (-40.7 ~ +63.7 s) |
| 1/14 Hz | | 23:38:01.4 (-47.5 ~ +35.2 s) |
| 1/12 Hz | | 23:38:08.2 (-73.2 ~ +66.4 s) |
| R1_1 | | |
| 1/14 Hz | | 23:33:33.0 (-36.1 ~ +25.9 s) |
| 1/12 Hz | | 23:33:59.4 (-19.8 ~ +17.6 s) |
| 1/10 Hz | | 23:34:09.1 (-19.4 ~ +10.6 s) |
| 1/8.4 Hz | | 23:34:12.6 (-21.6 ~ +11.9 s) |
| 1/7 Hz | | 23:34:23.2 (-11.9 ~ +15.0 s) |
| 1/6 Hz | | 23:34:23.6 (-11.9 ~ +10.1 s) |
| 1/5 Hz | | 23:34:24.9 (-14.0 ~ +15.4 s) |
| 1/4.2 Hz | | 23:34:25.8 (-10 ~ +11.21 s) |
| 1/3.5 Hz | | 23:34:26.0 (-8.8 ~ +9.4 s) |
| R2 | | |
| 1/34 Hz | | 01:14:05 (-70.5 ~ +66.6 s) |
| 1/28 Hz | | 01:13:49.4 (-62.7 ~ +43.1 s) |
| R3 | | |
| 1/34 Hz | | 01:38:57.5 (-340.8 ~ +78.3 s) |
| 1/28 Hz | | 01:39:17.1 (-141 ~ +66.6 s) |
| G1 | | |
| 1/48 Hz | | 23:33:38.2 (-84.7 ~ +103.0 s) |
| 1/40 Hz | | 23:33:38.2 (-84.7 ~ +53.2 s) |
| 1/34 Hz | | 23:33:38.2 (-70.0 ~ +104.7 s) |
| 1/28 Hz | | 23:34:03.1 (-131.3 ~ +156.2 s) |
| 1/24 Hz | | 23:34:04.9 (-51.0 ~ +31.3 s) |
| 1/20 Hz | | 23:34:23.0 (-70.8 ~ +52.7 s) |
| 1/17 Hz | | 23:34:31.2 (-32.9 ~ +29.6 s) |
| 1/14 Hz | | 23:34:36.1 (-39.5 ~ +42.8 s) |
| 1/12 Hz | | 23:34:20.3 (-26.7 ~ +31.3 s) |
| G1_-1 | | |
| 1/12 Hz | | 23:33:33.9 (-16.8 ~ +12.2 s) |
| 1/10 Hz | | 23:33:40.0 (-19.0 ~ +18.2 s) |
| 1/8.4 Hz | | 23:33:41.4 (-17.4 ~ +31.0 s) |
| 1/7 Hz | | 23:33:48.4 (-14.7 ~ +28.9 s) |
| 1/6 Hz | | 23:34:17.8 (-11.0 ~ +13.5 s) |
| 1/5 Hz | | 23:34:19.8 (14.6 ~ +31.9 s) |
| x4 | | 03:16:43.3 (±60 s) |
| x5 | | 03:42:00.6 (±60 s) |

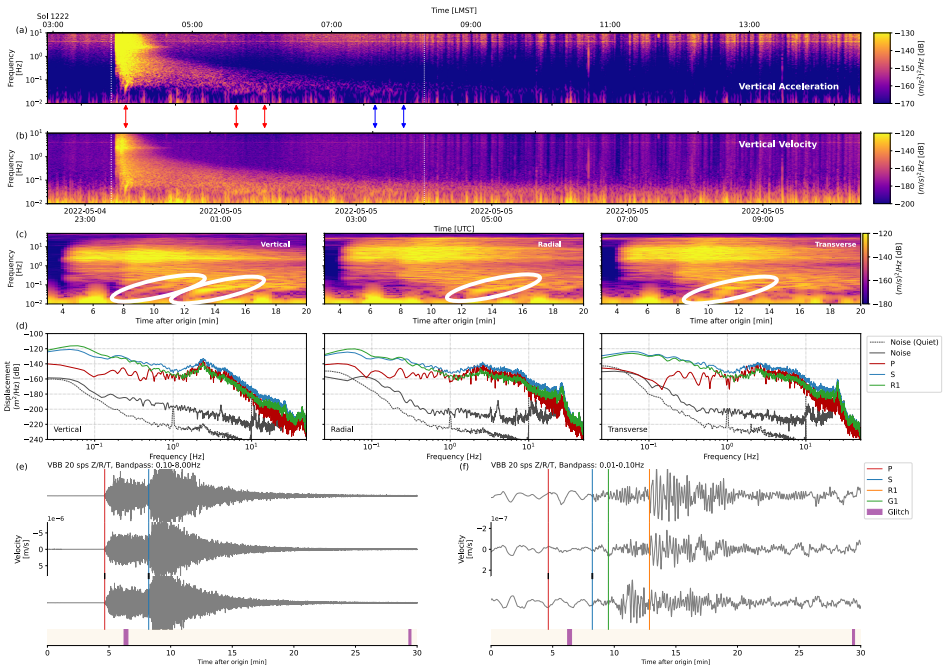


Figure 1: Event summary for S1222a. (a) 12 hour spectrogram in acceleration on the long period signal of the event. 20Hz deglichted data was used for the plot. Time window of 200 second with 90% overlap was used. The 3 red arrows below indicate R1/2/3 arrivals from the MQS catalog and the 2 blue arrows correspond to the x4 and x5 arrivals. The white dotted line is the origin time and the event end time from the catalog. (b) 12 hour spectrogram in velocity including the high frequency energy. The same time window and overlap as (a) was used. (c) 3 axes velocity spectrogram zoomed in to the event and expanded to the full frequency band width. 100 Hz deglichted data were used for the plot. Time window of 100 seconds and overlap of 90% were used. (d) Spectra of P, S and R1 energy of the event compared with pre-event noise and the noise level of a quiet period during the mission (noise curve of Sol 0235 were taken). To calculate P and S spectra, spectral time windows in the MQS catalog were used. For the noise, we also referred to the noise window in the catalog. For the noise level of the quiet season, we took noise window of marsquake S0235b. (e) Seismograms filtered between 0.1-0.8 Hz. The red and the blue lines refer to P and S arrival times identified by MQS. Glitches identified by MQS are indicated in purple in the bottom.(f) Seismograms filtered between 0.01-0.1 Hz. The red and blue lines refer to P and S arrival times identified by MQS. Arrival times of fundamental Rayleigh and Love waves are shown in orange and green. For the surface waves the earliest arrival of all the frequency bands is shown in the figure. For (c)-(f), the signal were rotated to vertical, radial and transverse component using the back-azimuth we obtained

(Table1).

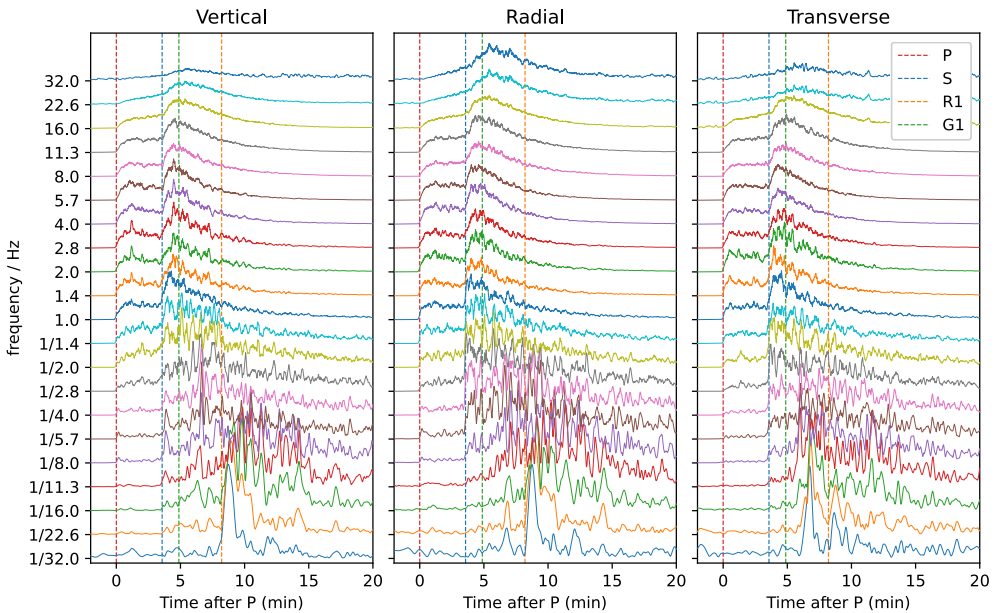


Figure 2: Filterbanks of S1222a. To create the filterbanks, both 20 Hz and 100 Hz data were used. Frequencies above 10 Hz used 100 Hz channels and were deglitched using the seisdeglitch tool (<https://pss-gitlab.math.univ-paris-diderot.fr/data-processing-wg/seisglitch>). The low frequencies below 10 Hz used 20 Hz continuous VBB channels and were deglitched with the method developed in UCLA (see Scholz et al. (2020) for further details) which achieves more efficient deglitching but is not applicable to 100 Hz data. The deglitching was tailored specifically for the event and was more efficient in removing glitches within the P and S code. Each trace shows the filtered envelope smoothed with 10 second time window. Each trace is bandpass-filtered at the frequencies shown in the y-axis. The filters are half an octave wide on each side. Body (P and S) and surface wave (Rayleigh and Love) arrivals are indicated with vertical dashed lines.

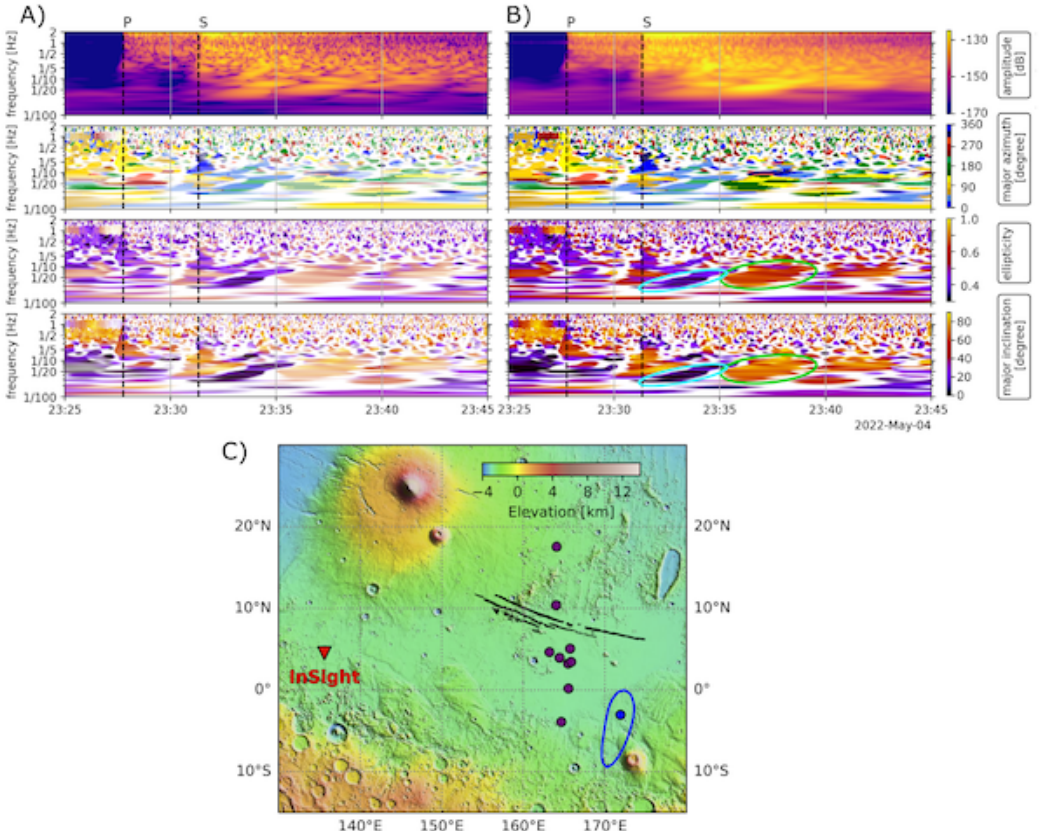


Figure 3: Polarisation and location of S1222a. (a) Data filtered to enhance linear, polarised signals. (b) Data filtered to enhance only polarised data, no linearity filter. Love and Rayleigh waves with overtones are visible after the S wave pick. For both (a) and (b): Back Azimuth of S1222a obtained from eigenvector methods (Zenhäusern et al., 2022) using de-glitched data; time-frequency depiction of (top row) amplitude, (second row) azimuth, (third row) ellipticity, and (bottom row) inclination. (c) Shown are quality A event locations (purple dots) and the InSight location (red triangle). The location of S1222a is marked by the blue uncertainty ellipse with a blue dot to show the preferred location. The Cerberus Fossae graben are marked with black lines. Updated from (Zenhäusern et al., 2022). The map background uses Mars Orbiter Laser Altimeter elevation data (Smith et al., 2001).

364 References

- Banerdt, W. B., Smrekar, S. E., Banfield, D., Giardini, D., Golombek, M., Johnson, C. L., ... Wieczorek, M. (2020). Initial results from the InSight mission on Mars. *Nat. Geosci.*, *13*(3), 183–189. doi: 10.1038/s41561-020-0544-y
- Banfield, D., Rodriguez-Manfredi, J. A., Russell, C. T., Rowe, K. M., Leneman, D., Lai, H. R., ... Banerdt, W. B. (2019). InSight Auxiliary Payload Sensor Suite (APSS). *Space Sci. Rev.*, *215*(1), 4. doi: 10.1007/s11214-018-0570-x
- Banfield, D., Spiga, A., Newman, C., Forget, F., Lemmon, M., Lorenz, R., ... Banerdt, W. B. (2020). The atmosphere of Mars as observed by InSight. *Nat. Geosci.*, *13*(3), 190–198. doi: 10.1038/s41561-020-0534-0
- Beghein, C., Li, J., Weidner, E., Maguire, R., Wookey, J., Lekić, V., ... Banerdt, W. (submitted). Structure along the martian dichotomy constrained by rayleigh and love waves and their overtones. *Geophysical Research Letters*.
- Böse, M., Clinton, J. F., Ceylan, S., Euchner, F., van Driel, M., Khan, A., ... Banerdt, W. B. (2017). A probabilistic framework for single-station location of seismicity on Earth and Mars. *Phys. Earth Planet. Inter.*, *262*, 48–65. doi: <https://doi.org/10.1016/j.pepi.2016.11.003>
- Böse, M., Stähler, S. C., Deichmann, N., Giardini, D., Clinton, J., Lognonné, P., ... Banerdt, W. B. (2021, Jun 22). Magnitude scales for marsquakes calibrated from insight data. *Bull. Seismol. Soc. Am.*. doi: 10.1785/0120210045
- Brinkman, N., Stähler, S. C., Giardini, D., Schmelzbach, C., Khan, A., Jacob, A., ... Banerdt, W. B. (2021). First focal mechanisms of marsquakes. *J. Geophys. Res.: Planets*, *126*(4), e2020JE006546. doi: <https://doi.org/10.1029/2020JE006546>
- Ceylan, S., Clinton, J. F., Giardini, D., Böse, M., Charalambous, C., van Driel, M., ... Perrin, C. (2021). Companion guide to the marsquake catalog from InSight, Sols 0–478: Data content and non-seismic events. *Phys. Earth Planet. Inter.*, *310*, 106597. doi: <https://doi.org/10.1016/j.pepi.2020.106597>
- Ceylan, S., Clinton, J. F., Giardini, D., Stähler, S. C., Horleston, A., Kawamura, T., ... Banerdt, W. B. (2022). The marsquake catalogue from insight, sols 0–1011. *Phys. Earth Planet. Inter.*, *106943*. doi: 10.1016/j.pepi.2022.106943
- Charalambous, C., Stott, A. E., Pike, W. T., McClean, J. B., Warren, T., Spiga, A., ... Banerdt, W. B. (2021). A comodulation analysis of atmospheric energy injection into the ground motion at insight, mars. *J. Geophys. Res.: Planets*, *126*(4), e2020JE006538. doi: <https://doi.org/10.1029/2020JE006538>
- Clinton, J. F., Ceylan, S., van Driel, M., Giardini, D., Stähler, S. C., Böse, M., ... Stott, A. E. (2021). The marsquake catalogue from insight, sols 0–478. *Phys. Earth Planet. Inter.*, *310*, 106595. doi: <https://doi.org/10.1016/j.pepi.2020.106595>
- Clinton, J. F., Giardini, D., Lognonné, P., Banerdt, B., van Driel, M., Drilleau, M., ... Spiga, A. (2017, 07). Preparing for InSight: An Invitation to Participate in a Blind Test for Martian Seismicity. *Seismological Research Letters*, *88*(5), 1290–1302. Retrieved from <https://doi.org/10.1785/0220170094> doi: 10.1785/0220170094
- Dahmen, N. L., Zenhäusern, G., Clinton, J. F., Giardini, D., Stähler, S. C., Ceylan, S., ... Banerdt, W. B. (2021, 10). Resonances and Lander Modes Observed by InSight on Mars (1–9 Hz). *Bull. Seismol. Soc. Am.*, *111*(6), 2924–2950. doi: 10.1785/0120210056
- Drilleau, M., Samuel, H., Garcia, R. F., Rivoldini, A., Perrin, C., Michaut, C., ... Banerdt, W. B. (2022). Marsquake locations and 1-d seismic models for mars from insight data. *Journal of Geophysical Research: Planets*, *127*(9), e2021JE007067. Retrieved from <https://agupubs.onlinelibrary.wiley.com/doi/abs/10.1029/2021JE007067> (e2021JE007067 2021JE007067) doi: <https://doi.org/10.1029/2021JE007067>
- Drilleau, M., Samuel, H., Rivoldini, A., Panning, M., & Lognonné, P. (2021, 03).

- 418 Bayesian inversion of the Martian structure using geodynamic constraints. *Geo-*
 419 *phys. J. Int.*, 226(3), 1615–1644. doi: 10.1093/gji/ggab105
- 420 Garcia, R. F., Daubar, I. J., Beucler, É., Posiolova, L. V., Collins, G. S., Lognonné,
 421 P., ... Banerdt, W. B. (2022, Sep 19). Newly formed craters on mars lo-
 422 cated using seismic and acoustic wave data from insight. *Nature Geoscience*.
 423 Retrieved from <https://doi.org/10.1038/s41561-022-01014-0> doi:
 424 10.1038/s41561-022-01014-0
- 425 Giardini, D., Lognonné, P., Banerdt, W. B., Pike, W. T., Christensen, U., Cey-
 426 lan, S., ... Yana, C. (2020). The Seismicity of Mars. *Nat. Geosci.* doi:
 427 10.1038/s41561-020-0539-8
- 428 Hobiger, M., Hallo, M., Schmelzbach, C., Stähler, S. C., Fäh, D., Giardini, D., ...
 429 Banerdt, W. B. (2021, Nov 23). The shallow structure of mars at the insight
 430 landing site from inversion of ambient vibrations. *Nature Communications*, 12(1),
 431 6756. doi: 10.1038/s41467-021-26957-7
- 432 Horleston, A., Clinton, J., Ceylan, S., Giardini, D., Charalambous, C., Irving, J., ...
 433 Banerdt, W. (2022). The far side of Mars: two distant marsquakes detected by
 434 InSight. *The Seismic Record*. doi: 10.1785/0320220007
- 435 InSight Mars SEIS Data Service. (2019). *Seis raw data, insight mission*. IPGP, JPL,
 436 CNES, ETHZ, ICL, MPS, ISAE-Supaero, LPG, MFSC. Retrieved from https://datacenter.ipgp.fr/networks/detail/XB_2016/ doi: 10.18715/SEIS.INSIGHT
 437 .XB_2016
- 438 Jacob, A., Plasman, M., Perrin, C., Fuji, N., Lognonné, P., Xu, Z., ... Banerdt,
 439 W. (2022). Seismic sources of insight marsquakes and seismotectonic con-
 440 text of elysium planitia, mars. *Tectonophysics*, 837, 229434. Retrieved from
 441 <https://www.sciencedirect.com/science/article/pii/S0040195122002281>
 442 doi: <https://doi.org/10.1016/j.tecto.2022.229434>
- 443 Johnson, C. L., Mittelholz, A., Langlais, B., Russell, C. T., Ansan, V., Banfield,
 444 D., ... Banerdt, W. B. (2020, 3). Crustal and time-varying magnetic fields
 445 at the InSight landing site on Mars. *Nature Geoscience*, 13(3), 199–204. doi:
 446 10.1038/s41561-020-0537-x
- 447 Karakostas, F., Schmerr, N., Maguire, R., Huang, Q., Kim, D., Lekic, V., ...
 448 Banerdt, B. (2021, 10). Scattering Attenuation of the Martian Interior through
 449 Coda-Wave Analysis. *Bulletin of the Seismological Society of America*, 111(6),
 450 3035–3054. Retrieved from <https://doi.org/10.1785/0120210253> doi:
 451 10.1785/0120210253
- 452 Khan, A., Ceylan, S., van Driel, M., Giardini, D., Lognonné, P., Samuel, H., ...
 453 Banerdt, W. B. (2021). Upper mantle structure of Mars from InSight seismic
 454 data. *Science*, 373(6553), 434–438. doi: 10.1126/science.abf2966
- 455 Kim, D., Banerdt, W. B., Ceylan, S., Giardini, D., Lekić, V., Lognonné, P., ...
 456 Panning, M. P. (2022). Surface waves and crustal structure on mars. *Sci-
 457 ence*, 378(6618), 417–421. Retrieved from <https://www.science.org/doi/abs/10.1126/science.abq7157> doi: 10.1126/science.abq7157
- 458 Kim, D., Davis, P., Lekić, V., Maguire, R., Compaire, N., Schimmel, M., ...
 459 Banerdt, W. B. (2021, 10). Potential Pitfalls in the Analysis and Structural
 460 Interpretation of Seismic Data from the Mars InSight Mission. *Bull. Seismol. Soc.
 461 Am.*, 111(6), 2982–3002. doi: 10.1785/0120210123
- 462 Kim, D., Lekić, V., Irving, J. C. E., Schmerr, N., Knapmeyer-Endrun, B., Joshi,
 463 R., ... Banerdt, W. B. (2021). Improving constraints on planetary interiors
 464 with pps receiver functions. *Journal of Geophysical Research: Planets*, 126(11),
 465 e2021JE006983. Retrieved from <https://agupubs.onlinelibrary.wiley.com/doi/abs/10.1029/2021JE006983> (e2021JE006983 2021JE006983) doi:
 466 <https://doi.org/10.1029/2021JE006983>
- 467 Kim, D., Stähler, S. C., Ceylan, S., Lekic, V., Maguire, R., Zenhäusern, G., ...
 468 Banerdt, W. B. (submitted). Structure along the martian dichotomy constrained

- 472 by rayleigh and love waves and their overtones. *Geophysical Research Letters*.
- 473 Knapmeyer-Endrun, B., Panning, M. P., Bissig, F., Joshi, R., Khan, A., Kim, D., ...
- 474 Banerdt, W. B. (2021). Thickness and structure of the martian crust from insight
- 475 seismic data. *Science*, 373(6553), 438–443. doi: 10.1126/science.abf8966
- 476 Li, J., Beghein, C., Lognonné, P., McLennan, S. M., Wieczorek, M., Panning, M., ...
- 477 Banerdt, W. B. (submitted). Analysis of minor- and major-arc rayleigh waves on
- 478 mars across the crustal dichotomy boundary. *Geophysical Research Letters*.
- 479 Lognonné, P., Banerdt, W., Pike, W., Giardini, D., Christensen, U., Garcia, R., ...
- 480 Zweifel, P. (2020). Constraints on the shallow elastic and anelastic structure of
- 481 Mars from InSight seismic data. *Nat. Geosci.*. doi: 10.1038/s41561-020-0536-y
- 482 Lognonné, P., Banerdt, W., Giardini, D., Pike, W., Christensen, U., Laudet, P., ...
- 483 Wookey, J. (2019). SEIS: Insight's Seismic Experiment for Internal Structure of
- 484 Mars. *Space Sci. Rev.*, 215(1), 12. doi: 10.1007/s11214-018-0574-6
- 485 Menina, S., Margerin, L., Kawamura, T., Lognonné, P., Marti, J., Drilleau, M., ...
- 486 Banerdt, W. B. (2021, 11). Energy Envelope and Attenuation Characteristics
- 487 of High-Frequency (HF) and Very-High-Frequency (VF) Martian Events. *Bulletin of the Seismological Society of America*, 111(6), 3016–3034. Retrieved from
- 488 <https://doi.org/10.1785/0120210127> doi: 10.1785/0120210127
- 489 Panning, M. P., Banerdt, W. B., Beghein, C., Carrasco, S., Ceylan, S., F., J., ...
- 490 ahler, S. C. S. (submitted). Locating the largest event observed on mars with
- 491 multi-orbit surface waves. *Geophysical Research Letters*.
- 492 Panning, M. P., Beucler, E., Drilleau, M., Mocquet, A., Lognonné, P., & Banerdt,
- 493 W. B. (2015). Verifying single-station seismic approaches using Earth-based data:
- 494 Preparation for data return from the InSight mission to Mars. *Icarus*, 248, 230 -
- 495 242. doi: 10.1016/j.icarus.2014.10.035
- 496 Perrin, C., Jacob, A., Lucas, A., Myhill, R., Hauber, E., Batov, A., ... Fuji, N.
- 497 (2022). Geometry and segmentation of cerberus fossae, mars: Implications for
- 498 marsquake properties. *J. Geophys. Res.: Planets*, 127(1), e2021JE007118. doi:
- 499 <https://doi.org/10.1029/2021JE007118>
- 500 Posiolova, L. V., Lognonné, P., Banerdt, W. B., Clinton, J., Collins, G. S., Kawa-
- 501 mura, T., ... Zenhäusern, G. (2022). Largest recent impact craters on mars:
- 502 Orbital imaging and surface seismic co-investigation. *Science*, 378(6618), 412–417.
- 503 Retrieved from <https://www.science.org/doi/abs/10.1126/science.abq7704>
- 504 doi: 10.1126/science.abq7704
- 505 Rivas-Dorado, S., Ruíz, J., & Romeo, I. (2022). Giant dikes and dike-induced seis-
- 506 micity in a weak crust underneath cerberus fossae, mars. *Earth and Planetary*
- 507 *Science Letters*, 594, 117692. Retrieved from <https://www.sciencedirect.com/science/article/pii/S0012821X22003284> doi: <https://doi.org/10.1016/j.epsl.2022.117692>
- 508 Scholz, J.-R., Widmer-Schnidrig, R., Davis, P., Lognonné, P., Pinot, B., Garcia,
- 509 R. F., ... Banerdt, W. B. (2020). Detection, Analysis, and Removal of Glitches
- 510 From InSight's Seismic Data From Mars. *Earth and Space Science*, 7(11),
- 511 e2020EA001317. doi: <https://doi.org/10.1029/2020EA001317>
- 512 Smith, D. E., Zuber, M. T., Frey, H. V., Garvin, J. B., Head, J. W., Muhleman,
- 513 D. O., ... Sun, X. (2001). Mars orbiter laser altimeter: Experiment summary af-
- 514 ter the first year of global mapping of mars. *J. Geophys. Res.: Planets*, 106(E10),
- 515 23689–23722. doi: <https://doi.org/10.1029/2000JE001364>
- 516 Stähler, S. C., Khan, A., Banerdt, W. B., Lognonné, P., Giardini, D., Ceylan, S., ...
- 517 Smrekar, S. E. (2021). Seismic detection of the martian core. *Science*, 373(6553),
- 518 443–448. doi: 10.1126/science.abi7730
- 519 Stähler, S. C., Mittelholz, A., Perrin, C., Kawamura, T., Kim, D., Knapmeyer, M.,
- 520 ... Banerdt, W. B. (2022, Oct 27). Tectonics of cerberus fossae unveiled by
- 521 marsquakes. *Nature Astronomy*. Retrieved from <https://doi.org/10.1038/s41550-022-01803-y> doi: 10.1038/s41550-022-01803-y

- 526 Stutzmann, E., Schimmel, M., Lognonné, P. H., Horleston, A. C., Ceylan, S., van
527 Driel, M., ... et al. (2020). Polarized ambient noise on mars. *Earth and Space*
528 *Science Open Archive*, 41. doi: 10.1002/essoar.10503376.1
- 529 van Driel, M., Ceylan, S., Clinton, J. F., Giardini, D., Alemany, H., Allam, A., ...
530 Zheng, Y. (2019). Preparing for InSight: Evaluation of the blind test for martian
531 seismicity. *Seismol. Res. Lett.*, 90(4). doi: <https://doi.org/10.1785/0220180379>
- 532 van Driel, M., Ceylan, S., Clinton, J. F., Giardini, D., Horleston, A., Margerin,
533 L., ... Banerdt, W. B. (2021). High-frequency seismic events on Mars ob-
534 served by InSight. *J. Geophys. Res.: Planets*, 126(2), e2020JE006670. doi:
535 <https://doi.org/10.1029/2020JE006670>
- 536 Zenhäusern, G., Stähler, S. C., Clinton, J. F., Giardini, D., Ceylan, S., & Garcia,
537 R. F. (2022). Low frequency marsquakes and where to find them: Back azimuth
538 determination using a polarization analysis approach. *Bull. Seismol. Soc. Am.*,
539 1–19. doi: 10.1785/01202220019
- 540 Zweifel, P., Mance, D., ten Pierick, J., Giardini, D., Schmelzbach, C., Haag, T., ...
541 Banerdt, W. B. (2021, 10). Seismic High-Resolution Acquisition Electronics for
542 the NASA InSight Mission on Mars. *Bull. Seismol. Soc. Am.*, 111(6), 2909–2923.
543 doi: 10.1785/0120210071